

Hybrid Quantum-Classical Reinforcement Learning in Latent Observation Spaces

Dániel T. R. Nagy^{1,2,3}, Csaba Czabán^{1,2,3}, Bence Bakó^{1,2,3}, Péter Hága³,
Zsófia Kallus³, Zoltán Zimborás^{1,2,4}

¹Eötvös Loránd University, Budapest, Hungary.

²HUN-REN Wigner Research Centre for Physics, Budapest, Hungary.

³Ericsson Research, Budapest, Hungary.

⁴Algorithmiq Ltd., Helsinki, Finland.

Email: nagy.dani@wigner.hun-ren.hu.

Abstract

Recent progress in quantum machine learning has sparked interest in using quantum methods to tackle classical control problems via quantum reinforcement learning. However, the classical reinforcement learning environments often scale to high dimensional problem spaces, which represents a challenge for the limited and costly resources available for quantum agent implementations. We propose to solve this dimensionality challenge by a classical autoencoder and a quantum agent together, where a compressed representation of observations is jointly learned in a hybrid training loop. The latent representation of such an autoencoder will serve as a tailored observation space best suited for both the control problem and the QPU architecture, aligning with the agent's requirements. A series of numerical experiments are designed for a performance analysis of the latent-space learning method. Results are presented for different control problems and for both photonic (continuous-variable) and qubit-based agents, to show how the QNN learning process is improved by the joint training.

Keywords: quantum machine learning, quantum reinforcement learning, hybrid training, autoencoders, latent space learning

1 Introduction

Machine learning (ML) solutions are rapidly adapted to many complex control applications requiring the modeling power of deep neural networks, e.g., of reinforcement learning (RL) agents. However, many of these application fields present problems where deep learning struggles with the complexity of hidden patterns leading to bottlenecks in performance and efficiency (Zubić et al.,

2024; Thompson et al., 2020). Thus, using accelerators and emerging technologies for ML efficiency improvement is an active field of research (Jouppi et al., 2023; Reuther et al., 2022).

One of these emerging technologies is quantum computing that can be adapted to classical problem spaces, acting as an accelerator. This approach is a rapidly growing sub-field of quantum machine learning (QML) (Huang et al., 2022; Xiao et al., 2023; Gyurik et al., 2022; Ristè et al., 2017).

Today, QML approaches can only be efficiently used as accelerators as part of hybrid solutions where the problem is jointly solved by quantum and classical parts.

As a part of this research area, Quantum Reinforcement Learning (QRL) is focusing on quantum algorithms for reinforcement learning models leveraging quantum computational resources (Kwak et al., 2021; Meyer et al., 2022). Current quantum processing units are however still limited in their scale and error tolerance (Bharti et al., 2022; Lau et al., 2022), therefore developing and testing heuristic QRL approaches with real-world applications remains a challenge. A key issue in many QRL methods is that several real-world problems require encoding high-dimensional feature vectors into the QPU’s initial quantum state.

To tackle the high dimensionality of feature vectors, classical deep learning pipelines often use Autoencoders (AEs) (Hinton and Salakhutdinov, 2006; Goodfellow et al., 2016) or Variational Autoencoders (VAEs) (Kingma and Welling, 2013; Kingma and Welling, 2019) to extract relevant low-dimensional features from high-dimensional complex problem spaces, and perform computations on the latent-space vectors. Prominent examples of this approach are latent diffusion models, in which images are compressed by using VAEs and generative modeling is performed on latent images (Rombach et al., 2022). AEs have also been successfully used in reinforcement learning tasks, e.g., the Dreamer model is used for learning a latent-space representations with a VAE and for policy optimization by latent trajectory imagination (Lange and Riedmiller, 2010; van Hoof et al., 2016; Hafner et al., 2019).

QRL agents have been recently used to solve standard baseline problems in classical control benchmark environments of both discrete and continuous action spaces (Dunjko et al., 2017; Lamata, 2021; Chen et al., 2022; Wu et al., 2020; Nagy et al., 2021). Furthermore, QRL has been tested in various, e.g., free-energy-based RL with quantum Boltzmann machines (Schenk et al., 2024), QRL with various dimensionality reduction methods (Andrés et al., 2023), evolutionary learning strategies using tensor network-variational quantum circuits (Chen et al., 2022), photonic QRL with photonic proximal policy optimization

(PPO) using on manual feature selection (Nagy et al., 2021).

In this paper, we present a method to train AEs and quantum agents jointly in a hybrid quantum-classical training loop such that the AE learns a particular feature extraction best suited for both the given problem and the QPU architecture.

The outline of this paper is as follows: in Section 2, we briefly review the ML and QML background of our work. Section 3 presents our novel method of training variational quantum agents based on parametrized quantum circuits (PQC) in latent observation spaces by using AEs and a combined loss function. In Section 4, we present the setup of our numerical experiments, while Section 5 discusses the obtained numerical results. Finally, in Section 6 we derive our conclusions and present some outlook for future work.

2 Background

In this section, we briefly review the technical background of our work, specifically, we review classical machine learning techniques of autoencoders and reinforcement learning, and also present the relevant methods of quantum reinforcement learning.

2.1 Autoencoders

Popular algorithmic feature reduction techniques such as Principal Component Analysis (PCA), Independent Component Analysis (ICA) or t-Distributed Stochastic Neighbor Embedding (t-SNE) are often unable to find the best low-dimensional features for high-complexity data, e.g., as visual data. To overcome this, deep neural network based feature reduction techniques such as AEs and VAEs have been implemented and are widely used to learn efficient dimensionality reductions on complex datasets, as well as mitigating or correcting specific noise and error patterns (Vincent et al., 2008; Yassenko et al., 2020; Restrepo et al., 2022).

AEs (Hinton and Salakhutdinov, 2006; Goodfellow et al., 2016) are a type of artificial neural network used in unsupervised machine learning and deep learning, primarily for data compression, feature learning, and dimensionality reduction.

The key idea behind AEs is to learn a compact representation (encoding) of input data by training the network to reconstruct its input as accurately as possible. AEs consist of an encoder $\mathcal{E} : \mathbb{R}^D \mapsto \mathbb{R}^L$, and a decoder $\mathcal{D} : \mathbb{R}^L \mapsto \mathbb{R}^D$. The encoder transforms data points $\mathbf{x} \in \mathbb{R}^D$ into a *latent space* representation $\mathbf{z} = \mathcal{E}(\mathbf{x}) \in \mathbb{R}^L$, whereas the decoder tries to reconstruct it: $\hat{\mathbf{x}} = \mathcal{D}(\mathbf{z})$. When $L < D$, the encoder produces a compact representation of the data. \mathcal{E} and \mathcal{D} are typically deep neural networks trained jointly via gradient descent optimization to minimize the reconstruction error or loss $\mathcal{L}(\mathbf{x}, \mathcal{D}(\mathcal{E}(\mathbf{x})))$. The loss function $\mathcal{L}(\mathbf{x}, \mathcal{D}(\mathcal{E}(\mathbf{x})))$ can be as simple as a mean-squared error (MSE) for continuous data (Goodfellow et al., 2016), categorical cross-entropy for categorical data (Goodfellow et al., 2016), or something more complex like Fréchet inception distance (FID) for visual data (Yu et al., 2021).

2.2 Classical reinforcement learning

Reinforcement Learning (RL) is a sub-field of machine learning aiming to train RL-*agents* such that these select the optimal *action* to be performed in an *environment*. Optimal actions maximize the cumulative *rewards* collected throughout the agents lifecycle. RL algorithms are either model-based, i.e., learning a predictive model of the environment, or model-free, i.e., learning a control policy directly without learning the underlying environment model.

Policy-based RL methods use a policy network π_θ , which defines an action probability distribution $\pi_\theta(\cdot|\mathbf{s}_t)$ over the space of allowed actions for every state \mathbf{s}_t of the environment.

At each timestep an action \mathbf{a}_t is sampled from the distribution $\pi_\theta(\cdot|\mathbf{s}_t)$ and executed in the environment, which in turn gives a scalar reward r_t as feedback. In general, a *trajectory* is defined as a sequence of states and actions $\tau = \{\mathbf{s}_1, \mathbf{a}_1, \dots, \mathbf{s}_T, \mathbf{a}_T\}$, and the corresponding trajectory reward is

$$R(\tau) = \sum_{t=1}^{\infty} \gamma^t r_t \approx \sum_{t=1}^T \gamma^t r_t, \quad (1)$$

with $\gamma \in (0, 1)$ being the discount factor. The general goal of RL is to find the optimal policy π_θ^*

which maximizes the expected trajectory reward:

$$\pi_\theta^* = \arg \max_{\pi_\theta} \mathbb{E}_{\tau \sim \pi_\theta} R(\tau). \quad (2)$$

To find the optimal policy, one usually estimates the expected return $\mathbb{E}_{\tau \sim \pi_\theta} R(\tau)$ and uses this to calculate the gradients $\nabla_{\theta} \mathbb{E}_{\tau \sim \pi_\theta} R(\tau)$ and perform gradient ascent optimization. This method is called the vanilla policy gradient (VPG) method (Sutton et al., 1999), which suffers from instability (Schulman et al., 2015, 2017), and hence other algorithms like proximal policy optimization (PPO) were invented.

Using the notation of (Schulman et al., 2017), here we briefly summarize the PPO algorithm. PPO is an RL algorithm designed to overcome the instability of VPG, by introducing a clipped surrogate objective. In order to do so, PPO calculates the probability ratios $r_t(\theta) = \pi_\theta(\mathbf{a}|\mathbf{s})/\pi_{\theta_{\text{old}}}(\mathbf{a}|\mathbf{s})$, and clips it outside the proximity region defined by ϵ as:

$$\text{clip}(r_t(\theta), \epsilon) = \begin{cases} 1 - \epsilon, & \text{if } r_t(\theta) < 1 - \epsilon \\ r_t(\theta), & \text{if } r_t(\theta) \in [1 - \epsilon, 1 + \epsilon] \\ 1 + \epsilon, & \text{if } r_t(\theta) > 1 + \epsilon \end{cases}$$

Furthermore, an *advantage* estimate \hat{A}_t is calculated which represents the advantage of the updated policy compared to the old policy. The clipped surrogate loss can be calculated as

$$\mathcal{L}^{\text{CLIP}}(\theta) = \mathbb{E}_t \left[\min \left(r_t(\theta) \hat{A}_t, \text{clip}(r_t(\theta), \epsilon) \hat{A}_t \right) \right],$$

where the advantages \hat{A}_t are calculated via generalized advantage estimation (Schulman et al., 2018):

$$\hat{A}_t = \sum_{l=0}^{T-t-1} (\gamma \lambda)^l \delta_{t+l}, \quad (3)$$

and $\delta_t = r_t + \gamma V^\pi(\mathbf{s}_{t+1}) - V^\pi(\mathbf{s}_t)$. The value function $V^\pi(\mathbf{s}_t)$ is a neural network separate from π_θ and is usually trained via mean-squared error loss:

$$\mathcal{L}^{VF} = \mathbb{E}_t \left[(V^\pi(\mathbf{s}_t) - V_{\text{target}}^\pi(\mathbf{s}_t))^2 \right]. \quad (4)$$

The clipped surrogate objective $\mathcal{L}^{\text{CLIP}}$ ensures that the agent does not suffer from destructively large updates during training. This however limits the exploration, as the agent might not be able

to explore better policies and solve the problem. To overcome the exploration issue, it is straightforward to incentivize exploration by adding a positive entropy term to the loss:

$$\mathcal{L}^{\text{PPO}} = - [\mathcal{L}^{\text{CLIP}}(\theta) + c_1 S[\pi_\theta] + c_2 \text{Reg}(\theta)], \quad (5)$$

where $\text{Reg}(\theta)$ is some regularization term, usually L^2 regularization, and $S[\pi_\theta]$ is the entropy of the policy. Note that we want to maximize the PPO objective via gradient ascent, however common AI software packages such as tensorflow perform gradient descent by default, hence the minus sign of the objective. Figure 1 summarizes the components of this complex classical PPO training loop.

2.3 Quantum reinforcement learning

Quantum Reinforcement Learning (QRL) is an emerging area of quantum computing and reinforcement learning that explores how quantum algorithms and quantum resources can be applied to enhance traditional reinforcement learning techniques (Saggio et al., 2021; Meyer et al., 2022). The state space of quantum circuits scales exponentially with the number of qubits/qumodes and hence quantum approaches potentially enable the solutions of machine learning problems that are intractable for classical computers.

Many QRL approaches are based on quantum neural networks (QNNs) in a hybrid quantum-classical training loop (Nagy et al., 2021; Kwak et al., 2021; Dunjko et al., 2017; Lamata, 2021; Wu et al., 2020; Chen et al., 2022; Coelho et al., 2024), other QRL approaches use Grover’s search algorithm (Dong et al., 2008; Li et al., 2020), quantum annealing (Nuzhin and Yudin, 2023) or other quantum algorithms (Sannia et al., 2023) to optimize agents. QNN-based RL agents use parametrized quantum circuits (PQCs) as their core component and optimize PQC parameters via classical algorithms such as gradient descent to reach an optimal reward score in a specific environment. In this case, the parameters of the PQC are stored in the memory of a classical device and the PQC is used to generate a quantum state that is measured to obtain an action as its output. The classical optimizer computes the PPO loss, from which one can compute the gradients of the PQC parameters using the quantum device. Once the

PQC gradients are calculated, the classical optimizer can compute the updated gate parameters for each quantum gate of the circuit and continue the training loop with the updated circuit.

Formally, a quantum neural network is a parametrized unitary operator $U(\boldsymbol{\theta})$ defined by a sequence of layers composed of quantum gates. This unitary is acting on the initial quantum state of the system, ρ_i , producing a final state $\rho_f = U(\boldsymbol{\theta})\rho_i U^\dagger(\boldsymbol{\theta})$. Subsequently, measurements are performed on ρ_f to obtain the QNN outputs. In the case of QNN-based RL agents, we need to embed the state \mathbf{x} of the system into the PQC. Assuming that each layer of the QNN has trainable parameters $\boldsymbol{\theta}_l$, we can define an encoding unitary $U_E(\mathbf{x})$ which encodes classical features. The total unitary applied to the initial state ρ_i is therefore

$$U(\{\boldsymbol{\theta}_l\}; \mathbf{x}) = \left(\prod_{l=1}^L U_L(\boldsymbol{\theta}_l) \right) U_E(\mathbf{x}), \quad (6)$$

where $U_L(\boldsymbol{\theta}_l)$ represents the trainable part of the l -th layer. In many cases, we want to apply the data re-uploading technique (Pérez-Salinas et al., 2020) to increase the performance and stability of the QNN during training. Data re-uploading means the repeated application of the encoding unitary U_E at the beginning of every quantum layer, thus leading to

$$U(\{\boldsymbol{\theta}_l\}; \mathbf{x}) = \prod_{l=1}^L (U_L(\boldsymbol{\theta}_l) U_E(\mathbf{x})). \quad (7)$$

Usually, we compute outcomes of multiple shots, i.e., we prepare N copies of the input quantum state ρ_i and produce N copies of the output state $\rho_{f,n}$ using the same PQC defined by $U(\boldsymbol{\theta}; \mathbf{x})$. To compute an action \mathbf{a} from these, we can perform the measurement Π on each of the N final states yielding N outcomes

$$y_n \sim \text{Tr}\{\Pi\rho_f\}. \quad (8)$$

Actions can be calculated from the measurement outcomes y_n with some post-measurement processing function f_{post} :

$$\mathbf{a} = f_{\text{post}}(y_1, y_2, \dots, y_N). \quad (9)$$

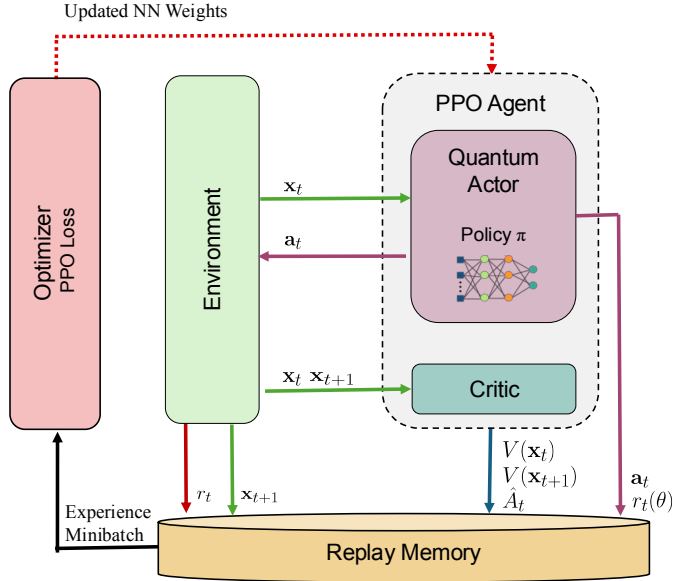


Figure 1: Classical PPO algorithm training loop. The PPO agent is composed of two neural networks: actor (a.k.a. policy) and critic. The policy network receives an observable from the environment and decides the actions to be performed. The critic network receives state vectors and computes the state values as well as the action advantages. Rewards, states, actions, values, advantages and policy ratios are stored in a replay memory, from which minibatches are sampled during training.

The selected actions are then executed in the classical environment leading to reward scores, and subsequently, the PPO loss $\mathcal{L}^{\text{PPO}}(\{\theta_l\})$ defined by Eq. 5 is calculated on a classical machine. The PPO loss is then used to compute updated PQC parameters via a gradient descent algorithm with learning rate α : $\theta_l \leftarrow \theta_l - \alpha \nabla_{\theta_l} \mathcal{L}^{\text{PPO}}$.

3 Hybrid QRL in adapted latent observation spaces

In this section, we introduce an end-to-end hybrid quantum-classical system and a training method for training and inference of QRL agents in classical RL environments with high dimensional observation spaces. The proposed system consists of a classical AE as a dimension reduction and feature extraction component, a QNN-based hybrid PPO agent with quantum policy and classical critic, and a classical optimizer which is jointly optimizing the parameters of both the quantum and the classical parts of the system for optimal decision making.

The key component is the joint training algorithm, which ensures that the AE learns a feature extraction which is specific to the given RL problem and QPU architecture. The proposed architecture enables NISQ quantum agents to be used in cases where the problem’s dimensionality and complexity would render simple QRL approaches infeasible. The proposed hybrid training loop and its key components are shown on Figure 2. While other works explored dimension reduction methods in the context of QRL (Chen et al., 2022; Andrés et al., 2023), a joint training of AEs and QRL agents in a hybrid quantum-classical training loop represents a novel solution to this problem.

Our method employs a PQC-based quantum agent π_{θ} defined with circuit architecture $U(\{\theta_l\}; \mathbf{x})$ as explained by Eq. 6 (or Eq. 7 with data re-uploading included), with trainable parameters $\{\theta_l\}$. Furthermore, we use an encoder network \mathcal{E} with trainable parameters $\theta_{\mathcal{E}}$ and a decoder network \mathcal{D} with trainable parameters $\theta_{\mathcal{D}}$. Figure 2 presents all of the components of the training loop for the proposed hybrid QRL model.

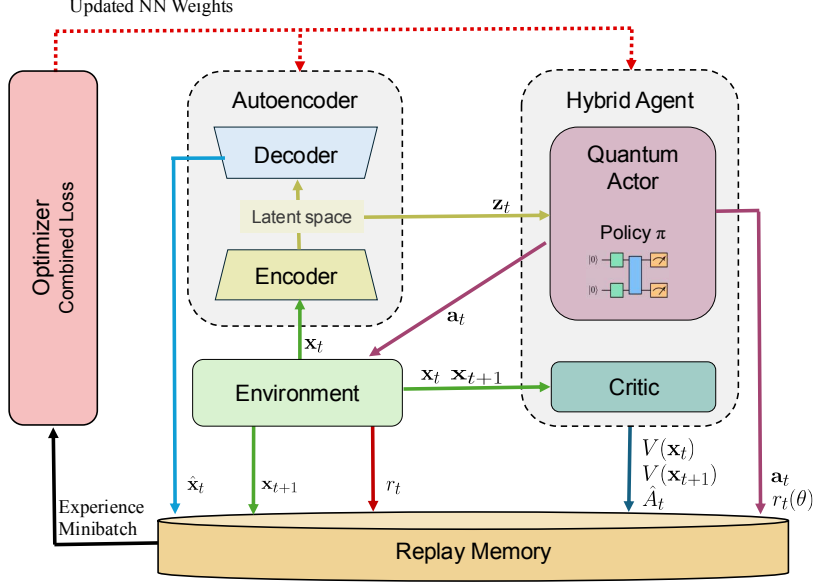


Figure 2: Hybrid quantum-classical QRL training via the PPO algorithm in latent observation space. An Autoencoder is introduced to learn latent state representation of a Classical Environment for optimal performance of a hybrid QRL PPO agent with quantum policy network. At each timestep, a Classical Optimizer updates the parameters for the Autoencoder and Quantum Policy networks based on a joint loss function. The Encoder \mathcal{E} compresses the observed state \mathbf{x}_t into a latent feature vector \mathbf{z}_t , that is passed to a Decoder \mathcal{D} . The reconstructed $\hat{\mathbf{x}}_t$ is used for calculating the loss function of the AE. The Quantum Policy π , i.e., the Actor of the QRL agent, will then choose best action \mathbf{a}_t based on the latent \mathbf{z}_t , yielding the reward r_t .

Joint training of the networks is implemented by calculating the weighted sum of PPO and AE losses with weight c_{AE} :

$$\mathcal{L} = \mathcal{L}^{\text{PPO}} + c_{AE}\mathcal{L}^{\text{AE}}. \quad (10)$$

The PPO loss \mathcal{L}^{PPO} is computed as in Eq. 5 and \mathcal{L}^{AE} is the AE loss suitable for the problem (e.g. MSE loss). Crucially, all trainable parameters $\{\theta_l\}, \theta_{\mathcal{E}}, \theta_{\mathcal{D}}$ are updated using the same optimizer, with gradients computed from the combined loss \mathcal{L} defined by Eq. 10:

$$\begin{aligned} \theta_l &\leftarrow \theta_l - \alpha \nabla_{\theta_l} \mathcal{L} \\ \theta_{\mathcal{E}} &\leftarrow \theta_{\mathcal{E}} - \alpha \nabla_{\theta_{\mathcal{E}}} \mathcal{L} \\ \theta_{\mathcal{D}} &\leftarrow \theta_{\mathcal{D}} - \alpha \nabla_{\theta_{\mathcal{D}}} \mathcal{L} \end{aligned}$$

During inference, only the (trained) encoder \mathcal{E} is used to compress feature vectors \mathbf{x}_t into latent features \mathbf{z}_t , which are used by the quantum policy π to generate actions \mathbf{a}_t . Optionally, it is possible to use pre-trained AEs and fine-tune them for

the given control task in the proposed hybrid RL training loop. This method is called *hot-starting* in contrast to starting with randomly initialized AE weights which is called *cold-starting*.

For complex feature vectors composed of different data types such as numeric, visual and categorical data, one can use separate AEs for each specific data type with their corresponding loss functions and weights contributing to the combined loss. In case of two or more AEs are used, all latent variables are encoded into the initial quantum state, with different suitable, encoding method.

4 Experiment design for hybrid latent-space QRL

We designed a series of numerical experiments to validate the proposed methods and demonstrate the advantages of the novel hybrid QRL

training approach. For that purpose, we integrated both classical environment simulators for RL optimization problems and QPU backend simulators for quantum circuit evaluations into ML libraries for gradient based training methods. The autoencoders were then easily integrated into this homogeneous software design through the underlying ML framework. In reason of computation resource efficiency, we designed minimal statistical ensemble training experiments where learning curve performance analysis can already show the characteristic differences between novel and existing methods.

4.1 Software integration

For the classical environment simulations, we used the RL benchmark environment API of the open-source Gymnasium (Towers et al., 2023). From the Gymnasium library we used the cart-pole problem, furthermore, we created a custom environment compatible with the Gymnasium API based on `numpy` for the visual navigation problem.

For the quantum computing simulations, we used both qubit-based and photonic architecture simulators compatible with state-of-the-art QML software frameworks, i.e., the PennyLane software framework (Bergholm et al., 2018) to implement qubit-based numerical experiments, and Piquasso photonic quantum simulation software platform (Kolarovszki et al., 2024) for continuous-variable QNN (CV-QNN) architectures (Killoran et al., 2019).

Both PennyLane and Piquasso implement QPU simulator backends that are compatible with TensorFlow (Abadi et al., 2016), i.e., the experiments can be run on GPUs within HPC clusters. Furthermore, both frameworks come with out-of-the-box methods for calculating quantum gradients of PQCs via parameter-shift rule for qubit-based circuits and finite difference method for photonic circuits. Alternatively, in these experiments we implemented the exact gradients with TF from the computational graph of circuits to achieve a significant speed-up of the simulations.

4.2 Dimension reduction

We test the proposed solution on the `CartPole-v1` (Figure 3 a.) and the `Maze-v0` (Figure 3 b.) environments, the former is part of Gymnasium, while the latter is a custom environment. Throughout

our experiments, we use fully connected AEs to compress the `CartPole-v1` observables and convolutional AEs for the `Maze-v0` environments, as these are better for visual data (Mao et al., 2016; Cheng et al., 2018). Table 1 summarizes these environments and their original feature space dimensionalities ($\dim(\mathbf{x})$) and the dimensions of the latent feature spaces ($\dim(\mathbf{z})$).

4.3 QRL agent circuit designs

The proposed latent observation space QRL method can be implemented across different quantum platforms and QPU architectures. To demonstrate this, we conduct numerical experiments using the two main approaches: qubit-based circuits and photonic (continuous-variable) quantum circuits. In this section we detail the QNN structure and measurement types for both of these architectures.

Qubit-based PPO agent design

For our qubit-based experiments, we use a QNN policy architecture based on strongly entangling layers as described in (Schuld et al., 2020). Such layers consist of a set of trainable rotation gates $R(\alpha, \beta, \gamma)$ applied to every qubit of the system, followed by a CNOT block to entangle qubits, then another set of rotation gates and finally a second CNOT block with different structure from the first one. These strongly entangling layers are repeated multiple times. To encode latent features, we use angle embedding, i.e., the encoding unitary is

$$U_E(\mathbf{z}) = \bigotimes_{j=1}^M R_Y^{(j)}(f_{\text{prep}}(z_j)), \quad (11)$$

where $R_Y^{(j)}$ denotes an Y -rotation applied to the j -th qubit of the system, and f_{prep} is some preprocessing function. Initially all qubits are in $|0\rangle$ state, and the angle-embedding U_E can be repeated at the beginning of every trainable layer as in (Pérez-Salinas et al., 2020). Crucially, the maximum dimension of latent feature vectors \mathbf{z} is limited by the number of qubits M . Figure 4 (a) shows the qubit based QNN architecture without data re-uploading.

To construct actions from the output quantum state, we estimate the expectation values $\langle Z_j \rangle$

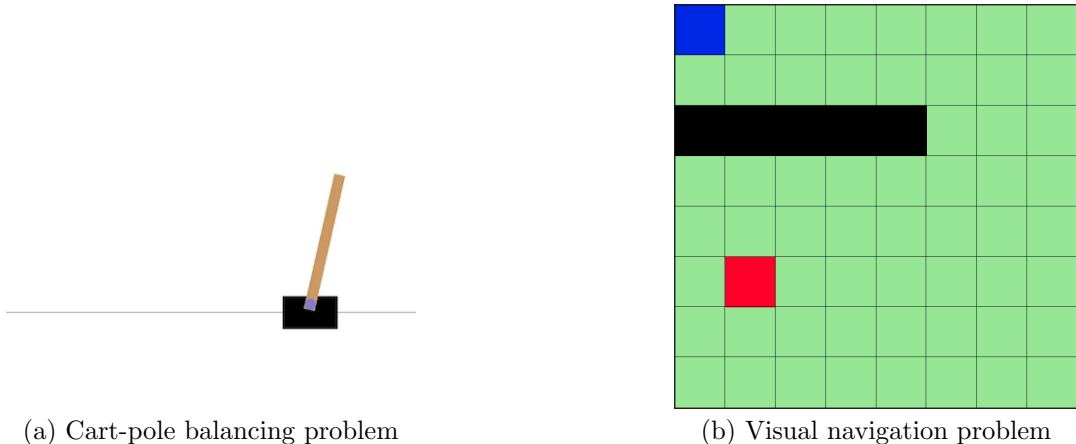


Figure 3: Optimal control problems used in this work. Two well-known classical simulated environments are selected for the numerical experiments. We used the OpenAI Gym protocol for the simulations during training of the hybrid QRL agents. **(a) Cart-pole balancing problem.** The goal is to keep the reverse pendulum from falling by applying left and right forces to the cart. Original observable state has 4 dimensions (cart position and velocity, pole angle and angular velocity), which we reduce to a 2-dimensional latent-space feature vector. **(b) Visual navigation problem.** The goal is to navigate the player (red square) to the target (blue square) while avoiding the walls (black squares). The agent receives the observable state as a 48×48 pixel sized grayscale image representing an 8×8 logical grid made from 6×6 pixel sized cells. We reduce this original feature vector to a 8-dimensional or 4-dimensional latent vector using a convolutional AE.

Environment	QC platform	$\dim(\mathbf{x})$	$\dim(\mathbf{z})$	Action space
CartPole-v1	qubit	4	2	Discrete(2)
Maze-v0	qubit	2304	8	Discrete(4)
CartPole-v1	qumode	4	2	Discrete(2)
Maze-v0	qumode	2304	6	Discrete(4)

Table 1: Simulated environments for different quantum computing platforms. $\dim(\mathbf{x})$ is the original observation space dimension as defined by the environment, $\dim(\mathbf{z})$ is the latent space dimension of the trained AE. Note that for the Maze-v0 environment, we use 8 qubits but only 6 qumodes, and hence the difference in $\dim(\mathbf{z})$. Each environment has a discrete action space with different number of possible actions.

for each qubit, and then construct the discrete probability distribution

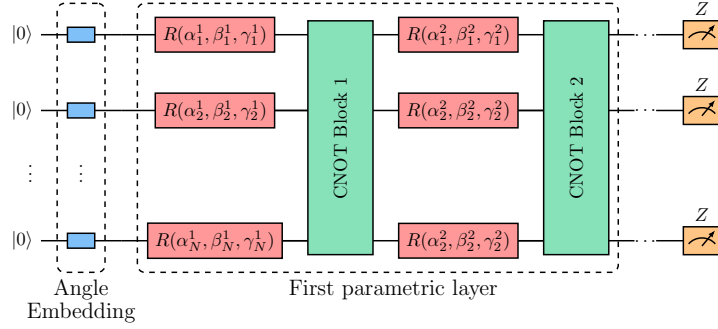
$$\Pr(a = j) = \frac{\exp\langle Z_j \rangle}{\sum_k \exp\langle Z_k \rangle}, \quad (12)$$

from which we sample actions a_t at each timestep.

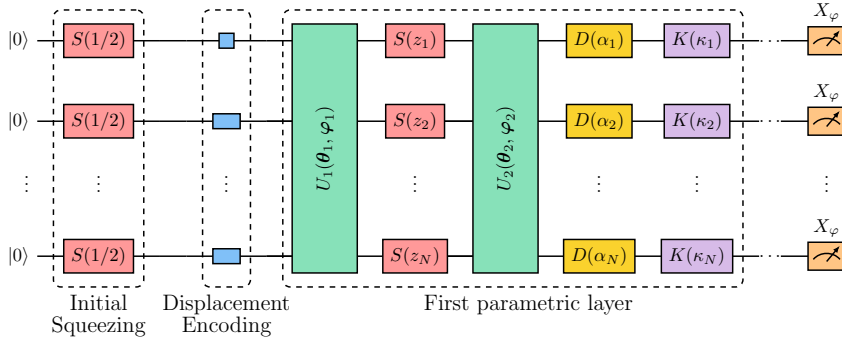
Photonic PPO agent design

Besides qubit-based QNNs, we also test our method with quantum policies implemented as

continuous variable QNNs (CV-QNNs), similarly to the numerical experiments presented in (Nagy et al., 2021). The CV-QNN Ansatz is composed of the following photonic gates: Gaussian gates including squeezing ($S(r, \phi)$), displacement $D(\alpha, \phi)$, and rotation ($R(\phi)$) a.k.a. phase-shifting; furthermore, in order to introduce non-linearity we need at least one nonlinear CV quantum gate (Killoran et al., 2019). We use Kerr-nonlinearities for this purpose ($K(\kappa)$). The general CV-QNN circuit architecture is shown on Figure 4 (b). In all



(a) Qubit-based circuit Ansatz for QRL



(b) Photonic circuit Ansatz for QRL Actor

Figure 4: QNN architectures for hybrid PPO policies. We used standard QNN architectures for the QRL Actor circuits. In both cases, the initial classical data encoding can be repeated with each layer, a technical method known as data re-uploading. **(a) Circuit Ansatz for the qubit-based policy.** Composed of an angle-embedding layer at the beginning of the circuit, followed by a number of standard strongly entangling trainable layers. **(b) Circuit Ansatz for the photonic policy.** Composed of an initialization by squeezing gates and displacement encoding layer followed by a number of trainable standard CV-QNN layers.

of the CV-QNN-based experiments, we use a pre-squeezed initial state i.e., we apply a squeezing of magnitude $1/2$ and phase $\pi/2$ to the M -mode vacuum state as initialization:

$$|\psi_i\rangle = S\left(\frac{1}{2}, \frac{\pi}{2}\right)^{\otimes M} |0^{\otimes M}\rangle. \quad (13)$$

Subsequently, we use displacement-encoding to encode latent features into the quantum state. Displacement-encoding applies a displacement of magnitude $f_{\text{prep}}(z_j)$ and phase $\pi/2$ to the j -th

mode of the CV quantum system:

$$U_E(\mathbf{z}) = \bigotimes_{j=1}^M D_j\left(f_{\text{prep}}(z_j), \frac{\pi}{2}\right), \quad (14)$$

where f_{prep} is some feature preprocessing function. f_{prep} can be the identity function, or an arctan-based preprocessing like in (Nagy et al., 2021):

$$f_{\text{prep}}(x) = \begin{cases} +\frac{4}{\pi} |\arctan(x)|^{1/3} & x > 0, \\ -\frac{4}{\pi} |\arctan(x)|^{1/3} & x < 0, \\ 0 & x = 0, \end{cases} \quad (15)$$

which ensures that the values of the displacement gate parameters remain reasonably small.

As in Eq. 7, the encoding unitary U_E can be repeated at the beginning of each trainable layer. The maximum number of modes M we can simulate limits the dimension of latent features \mathbf{z} that can be encoded into the system via displacement-encoding. A CV-QNN Ansatz without data re-uploading is shown on Figure 4 (b).

To construct actions from the output quantum state, we perform homodyne measurements and estimate the expectation values $\langle P_j \rangle$ for each qumode, and then construct the discrete probability distribution

$$\Pr(a = j) = \frac{\exp\langle P_j \rangle}{\sum_k \exp\langle P_k \rangle}, \quad (16)$$

from which we sample actions a_t at each timestep.

5 Evaluation of learning efficiency and performance

To enable performance comparison of training methods across different environments, we introduce a normalized version of the well-known area under learning curve (AULC) metric. First, we consider a normalized reward by the $P\%$ of the optimal score of the given environment. Second, we further normalize over the time dimension as well, i.e., the episode count, as follows: we consider the episode number e_P^E at which the best agent of the ensemble training for a given environment E reaches the previously set P percent of the optimal reward score. Hence the best agent will reach the maximal normalized reward of one at normalized episode number of one.

In this work, we apply this normalization technique over the averaged learning curves of an ensemble of agents, each also smoothed using a moving window average to counteract fluctuations.

Note that for complex learning curves, the AULC and normalized AULC scores could be misleading in itself, as it is reducing performance characteristics into a single number. Hence these results always need to be assessed together with the learning curves. Fast learning leads to a convex learning curve, i.e., a normalized AULC larger

than 0.5 while value under 0.5 could still reach P percent but with a slower initial learning and a concave learning curve.

Due to the stochastic nature of RL, it is required to average learning curves over multiple agents with the same hyper-parameters but initialized with different random seeds. We train 8 agents in parallel for each experiment, and we calculate performance metrics for 5 out of 8, as the outlier agents were discarded (usually without a visible learning trend).

5.1 Demonstration of the joint training method performance

First, we demonstrate a small-scale implementation of latent QRL training. We investigate whether the joint training of an AE and a QRL agent yields satisfactory agent performance results, and compare these with training a QRL agent using a pre-trained but fixed AE.

These tests were executed using both qubit-based and photonic QNN policies and on both the `CartPole-v1` and the `Maze-v0` environments. The learning ability of the joint training method is further evaluated by computing the normalized AULC metric for each training session, based on the 90% score thresholds.

Resulting learning curves are presented on Figures 5 (a) and (b) for qubit-based and photonic architectures respectively. Furthermore the computed normalized AULC scores are shown on Figures 5 (c) and (d) for qubit-based and photonic architectures respectively. Both the normalized learning curves and AULC scores indicate the necessity of joint training to achieve satisfactory learning performance: agents achieve at least 90% of the optimal score only when the joint training is applied. These results collectively show that the implementation of the proposed hybrid QRL agent with joint training is able to learn and solve RL problems even with high-dimensional observation spaces like `Maze-v0`.

Furthermore, results indicate that compared to the fixed pre-trained AE solution, the joint training approach shows better learning ability, and in some cases, it is able to solve RL problems that a fixed AE approach is unable to solve. Detailed description of the experiments and hyperparameters are summarized in Appendix A.

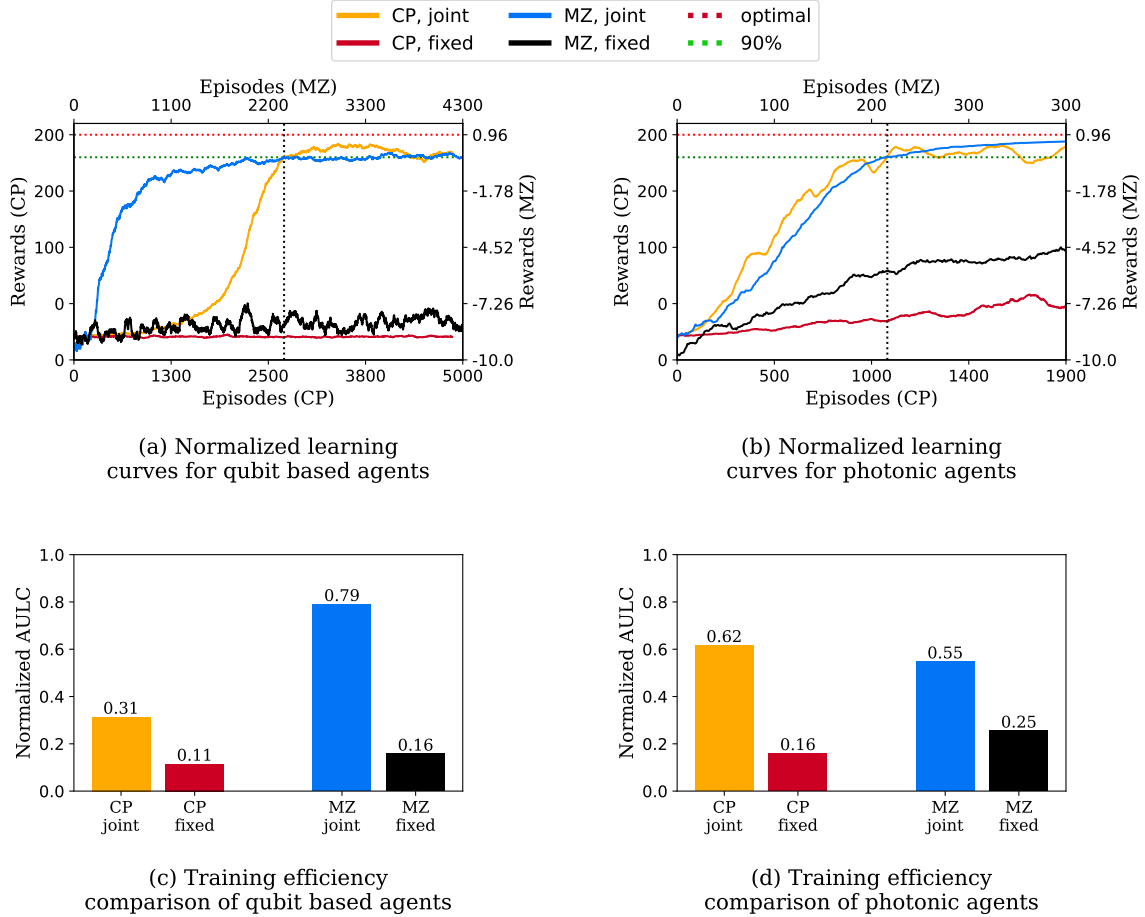


Figure 5: Performance evaluation of the novel latent-space QRL training method. We compare the novel latent-space training method via jointly trained AE for quantum policy against using a fixed AE for simple feature extraction. The results are shown for two types of QRL agent trained across two control problems: qubit-based and photonic agents in for the Cart-Pole balancing problem (`CartPole-v1` environment, labeled CP) and the visual navigation problem (`Maze-v0` environment, labeled MZ). **(a)-(b) Normalized learning curves.** Results show rewards normalized by each environment’s optimum. Learning curves are averaged over 8 agents, smoothed with 100-episode moving window. **(c)-(d) Training efficiency comparisons.** Results present the normalized area under learning curve (AULC) until faster training method reaches 90% of the normalized optimum. Higher values indicate faster convergence by episode normalization per environment, but we keep separate comparison per quantum agent type.

5.2 Exploration of AE compressive power vs QNN layer count

Besides testing the joint training method against a fixed AE solution, we also explore the interdependence between the size of the AE and the number of QNN layers. Balancing AE and quantum resources might be necessary because of compute resource limitations, or to maximize the utility of both quantum and classical resources.

Specifically, we use the `CartPole-v1` environment to assess how variations in the size of the AE and the number of QNN layers affect learning performance. Due to the computational cost of simulating photonic QNNs, this study is done using qubit-based policies only.

To explore the interdependence between AE and QNN complexities, we simulate a set of agents with various configurations as follows. We run a

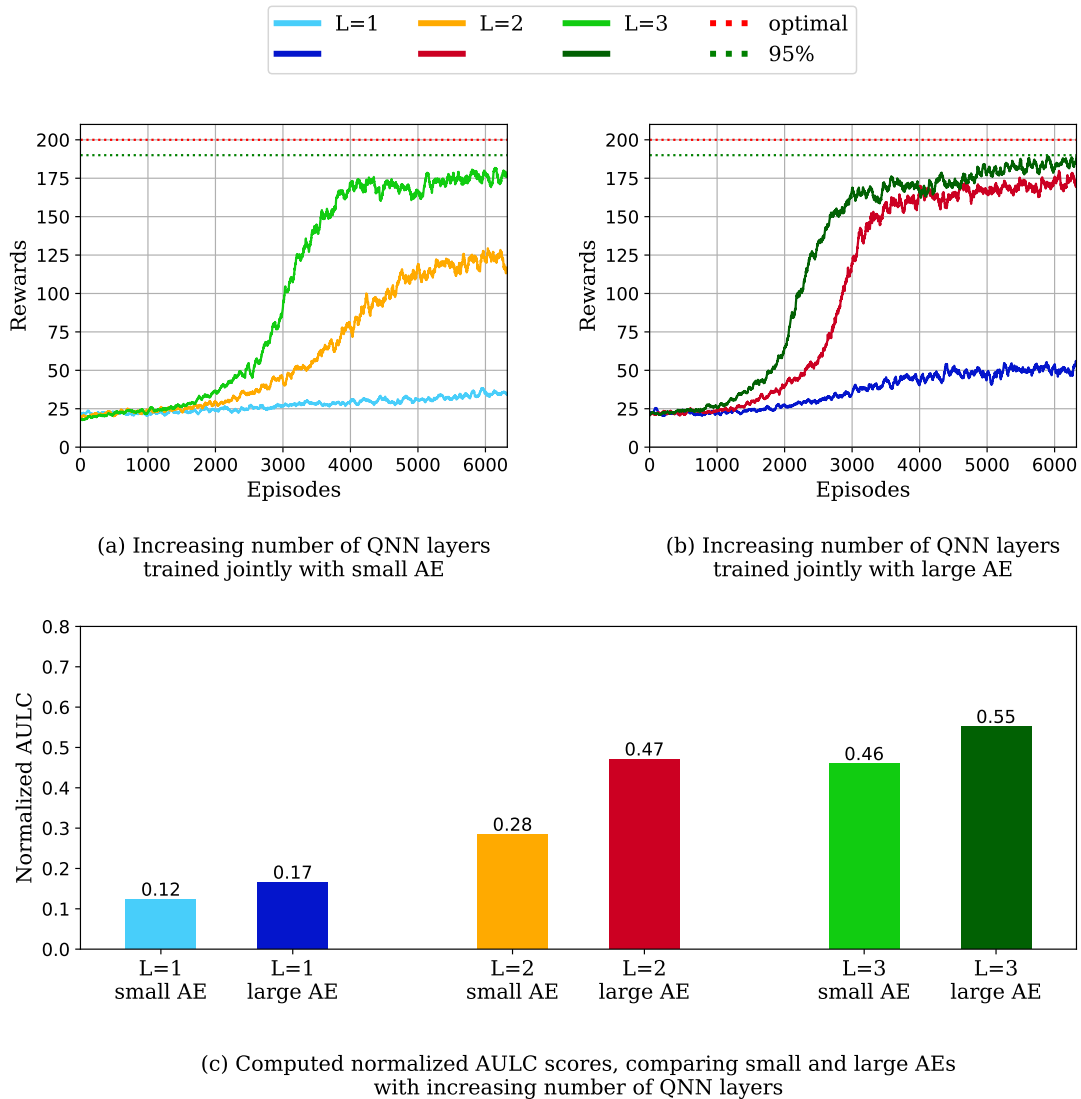


Figure 6: Learning power of hybrid agents: interdependence of QNN and AE complexity. Numerical experiments show that by increasing the number of AE parameters smaller QNN agents are enabled to reach better performance. Similarly, with increasing number of QNN layers, a smaller AE is sufficient for convergence. Results show that the minimal single-layer QNN agent is unable to learn even with large AE, however when we consider a two-layer QNN, using the larger AE enables satisfactory learning performance. For large QNNs, increasing the AE size does not yield significantly better results. Simulations were performed on the `CartPole-v1` environment using qubit-based agents.

number of training experiments in which we vary the number of QNN layers, with a fixed AE size. We repeat these simulations with a small AE and a larger AE configuration.

Learning curves for the small AE simulation are shown on Figure 6 (a) while Figure 6 (b) shows these in the case of the larger AE. Furthermore,

the computed the normalized AULC values in each case are shown on Figure 6 (c).

Results of these numerical experiments support our hypothesis that as the size of the AE increases, smaller QNN configurations yield improved performance, and similarly, as we increase the number of QNN layers, a smaller

AE is enough to achieve satisfactory learning performance. However due to the lack of computational resources, these experiments were only conducted on the `CartPole-v1` environment with qubit-based agents, thus finding whether a similar interdependence also exists in the case of the `Maze-v0` environment or in the case of photonic agents, further numerical experiments are required.

These results show that increasing the AE allows for a reduction in the number of QNN layers required, as expected. Furthermore, we find the limit of under-dimensioned QNN will not learn to solve the problem, not even with large AEs.

However, we find that there are limits to this trade-off: for instance, while a larger AE can compensate for fewer QNN layers to some extent, it is insufficient for extremely small QNN architectures such as single-layer QNNs. On the other hand, with an overdimensioned AE, independent of the QNN depth, the agent will remain classically determined, without performance explained by the QNN’s representative power. With balanced AE sizing, in the case of the `CartPole-v1` problem, we find that a minimum of three QNN layers is necessary to achieve satisfying learning results. Detailed description of the experiments and hyperparameters are summarized in Appendix A.

5.3 Benchmark results against classical baselines

To compare our solution with a fully classical counterpart, we choose the `Maze-v0` environment, as this is only solvable by a quantum agent when an AE is assisting with feature extraction due to the high dimensionality of the problem. Furthermore, this study uses photonic agents, as qubit-based agents with the shallow Ansatz configuration did not achieve near-optimal performance.

To compare the classical and hybrid solutions, the number of trainable parameters in the classical agent is adjusted so that the combined number of parameters in the QNN and the AE of the hybrid agent is approximately the same. Trainable parameter counts for each scenario are detailed in Appendix A.

Figures 7 (a) and (b) present the comparison of learning curves between a photonic quantum agent

assisted by a convolutional AE and a fully classical CNN-based agent. Configurations presented on Figures 7 (a) and (b) differ in the number of QNN layers used ($L = 3$ and $L = 6$ respectively), and the CNN parameter count is adjusted to the number of QNN params in each case.

Results show that the photonic agents achieve faster learning compared to a similarly sized fully classical agent. This is also confirmed by the computed normalized AULC scores shown on Figure 7 (c). Detailed description of the experiments and hyperparameters are summarized in Appendix A.

6 Conclusions and outlook

Quantum machine learning offers a way of using the powerful expressivity of quantum systems for classical problem solving. However, due to the scarcity of quantum resources, an essential challenge is to efficiently encode the high-dimensional descriptors of real-world problems for quantum agents. A natural way of addressing this challenge is to extract the task-specific information from the general descriptors. Since such problem representations are among the most fundamental building blocks on the path towards useful QML, this work focused on a novel solution for efficiently encoding high-dimensional observations into the initial quantum state of the QRL policy circuit Ansatz for optimal control performance.

In particular, we proposed integrating classical AEs with QRL agents in a joint hybrid quantum-classical training loop. This joint training ensures that the AE learns feature extraction tailored to the specific RL problem and QPU architecture, thereby leading to more efficient and effective learning.

We designed a series of experiments for the comparative analysis of the proposed method for two classical RL benchmark problems, the cart-pole balancing and a visual navigation problems. Using the particular `CartPole-v1` and `Maze-v0` environments, we implemented hybrid PPO agents in both qubit-based and photonic quantum circuits. The analysis showed that the joint training approach significantly outperforms the fixed pre-trained AE case in these two very distinct environments for qubit-based as well as photonic agents. In presenting the design of the numerical experiments, we also highlighted the

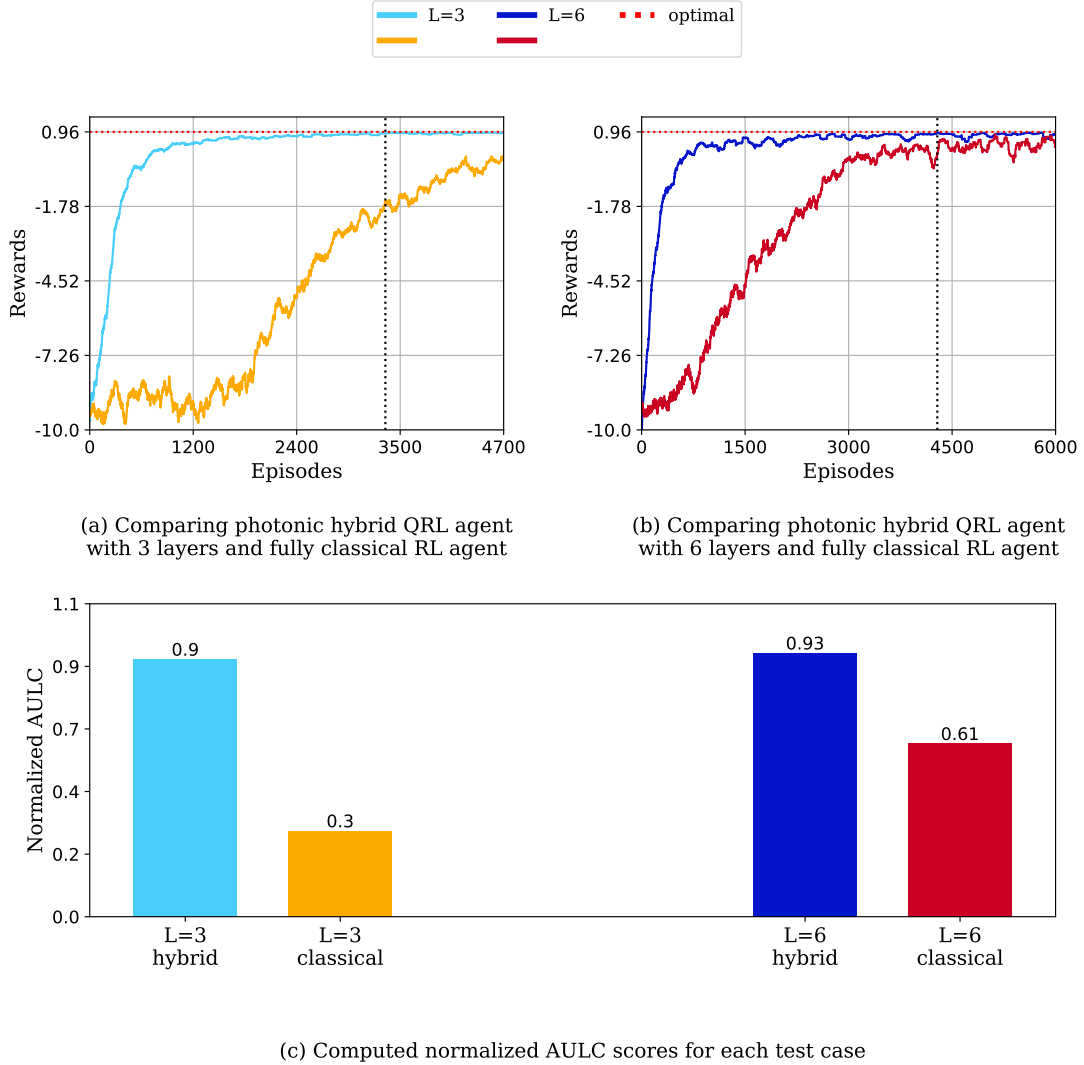


Figure 7: Comparison of fully classical and hybrid agents. Comparing learning curves for agents with similar parameter counts and hyperparameters and randomly initialized parameters. Figures show the smoothed learning curves averaged over 8 parallel agents. **(a)** - **(b)**: results for photonic QNN agents; **(c)** - **(d)**: results for qubit-based QNN agents. For shallow QNN-based agents, the difference between the hybrid solution and its classical counterpart seems larger than for deeper circuits.

importance of the interplay between the compressive power of the AE component and the control performance of the QNN agent - in relation to the specifics of each control environment.

Comparisons against fully classical agents in the *Maze-v0* environment revealed that our approach of joint training reaches similar solution quality with often a faster convergence. This effect was particularly pronounced in the photonic

QNN experiments. Throughout these comparative experiments, we trained agents with similar number of trainable parameters and similar hyperparameters.

The presented novel hybrid training method paves the way towards real-world problems where one could benefit from the expressive power of quantum agents. This initial study could be extended in multiple ways. We can generalize

the study by replacing simulators with QPU prototype hardware or testing the method in real environments. We can also extend the method towards more complex problem spaces, e.g., multi-modal observables or multi-agent scenarios, where each modality or agent will be trained with their own respective AEs. It would be interesting to see whether the observed faster convergence would also prevail in these situations.

Acknowledgment

Dániel T. R. Nagy, Bence Bakó, Zoltán Zimborás and Zsófia Kallus would like to thank the support provided by the Ministry of Culture and Innovation of Hungary from the National Research, Development and Innovation Fund (NKFIH), financed under the KDP-2021 and KDP-2023 funding schemes (Grants No. C1788111 and C2245275). Zoltán Zimborás would like to thank the support of the NKFIH through the Grants No. FK 135220 and TKP2021-NVA-29 and the Quantum Information National Laboratory of Hungary. The authors acknowledge the computational resources provided by the Wigner Scientific Computational Laboratory.

A Supplementary Information

In this section, we present supplementary information detailing the configurations utilized in our experiments with the `CartPole-v1` and `Maze-v0` environments. The tables provided here detail the QNN parameter counts for both qubit and qumode platforms as well as of the parameter counts for the classical fully connected and convolutional AEs. Furthermore, we detail the configurations and parameter counts of the fully classical CNN-based agents we use as baseline for the classical versus hybrid QRL comparisons.

Table 2 and Table 3 summarize the parameter counts for QNNs with different number of layers, distinguishing between the qubit-based and photonic agent approaches in both environments.

To investigate the interdependence of QNN layer count and AE param counts, we trained the hybrid QRL agent together with a small and a large AE using 1, 2 and 3 QNN layers. Table 4 contains the parameter counts for the small and large fully-connected AEs. The small AE consists of a single `Dense(2)` layer followed by a `sigmoid` activation, while the large AE consists of a `Dense(8)` and a `Dense(2)` layer, each followed by `sigmoid` activations. Both AEs are pretrained using a learning rate schedule defined by the `PiecewiseConstantDecay` class. The decay boundaries are set at 250, 500, 750, 1000, 1250, and 1500 epochs, with corresponding learning rate values of 0.05, 0.01, 0.005, 0.001, 0.0005, 0.0001, and 0.00005, respectively. Both AEs are trained for 20,000 epochs with a batch size of 16.

Table 5 details the hyperparameters of the convolutional AE used for the `Maze-v0` environment. This consists of two primary components: a convolutional encoder and a convolutional decoder. The encoder accepts input images with dimensions of 48x48 pixels and 1 channel, and encodes them into a latent space of 6 dimensions. The encoder employs `Conv2D` layers with filters set to [2, 4, 8, 8] and uses the `ReLU` activation function. There are no additional hidden layers in the encoder.

The decoder mirrors the encoder’s structure. It reconstructs the 48x48 pixel output images with 1 channel from the latent space representation. The decoder uses `Conv2DTranspose` filters set to [8, 8, 4, 2] and applies bilinear interpolation for upsampling. It also uses the `ReLU` activation function and includes no extra hidden layers.

Environment	platform	QNN layers	QNN params
CartPole-v1	qubit	1	6
CartPole-v1	qubit	2	12
CartPole-v1	qubit	3	18
CartPole-v1	qubit	6	32
CartPole-v1	qumode	1	14
CartPole-v1	qumode	3	42
CartPole-v1	qumode	6	84

Table 2: Parameter counts used in the CartPole-v1 problem. The table summarizes the number of layers and corresponding number of QNN parameters for both qubit-bases agents and photonic agents.

Environment	platform	QNN layers	QNN params
Maze-v0	qubit	1	24
Maze-v0	qubit	3	72
Maze-v0	qubit	5	120
Maze-v0	qumode	1	94
Maze-v0	qumode	3	282
Maze-v0	qumode	6	564

Table 3: Parameter counts used in the Maze-v0 problem. The table summarizes the number of layers and corresponding number of QNN parameters for both qubit-bases agents and photonic agents.

Environment	Name	Hidden Sizes	Encoder Params	Decoder Params
CartPole-v1	small AE	[2]	10	12
CartPole-v1	large AE	[8,2]	58	60

Table 4: Parameter counts for the fully connected AEs used in the CartPole-v1 experiments. The table summarizes the hidden layer configuration, encoder and decoder parameter counts for the small and large fully-connected AEs used in the CartPole-v1 experiments.

Name	Platform	Filter Sizes	Pooling size	Encoder Params	Decoder Params
convAE	qumode	[2, 2]	4	172	221
convAE	qubit	[2, 2]	4	210	257

Table 5: Parameter counts for the convolutional AE used in the Maze-v0 experiments. The table summarizes the number of parameters and filter configurations of the convolutional AE for both qubit based agents and photonic agents.

The convolutional AE is pretrained using the `PiecewiseConstantDecay` learning rate schedule, with boundaries at 250, 500, 750, 1000, 1250, and 1500 epochs. The corresponding learning rate values are 0.05, 0.01, 0.005, 0.001, 0.0005, 0.0001, and 0.00005, respectively. The convolutional AE is trained for 20,000 epochs with a batch size of 32.

The fully classical CNN agent has input observation space consisting of images with dimensions 48x48 pixels and 1 channel and outputs a 4-dimensional vector. The CNN consists of three convolutional layers, with filter sizes that vary depending on the specific configuration. The number of channels in the `Conv2D` layers are 8, 4,

Platform	Number of layers	CNN param count	convAE + QNN param count
qumode	1	519	487 (94 + 172 + 221)
qumode	3	731	675 (282 + 172 + 221)
qumode	6	974	957 (564 + 172 + 221)
qubit	1	517	491 (24 + 210 + 257)
qubit	3	556	539 (72 + 210 + 257)
qubit	5	609	587 (120 + 210 + 257)

Table 6: Parameter counts used in the classical vs quantum benchmark experiments on the Maze-v0 environment. The table summarizes parameter counts for the fully classical CNN agents, and parameter counts for the hybrid quantum-classical agents including the QNN and the classical convolutional AE.

and 3, respectively. After the Conv2D layers, the output is flattened, followed by a single hidden dense layer whose size also varies based on the chosen configuration. The agent uses the ReLU activation function throughout the network. Table 6 compares parameter counts of fully classical CNN agents against parameter counts of hybrid quantum-classical agents, we use in the classical versus hybrid QRL agent benchmark tests.

Hardware usage and code

Simulations were run on a hardware equipped with an Intel(R) Xeon(R) CPU E5-2650 CPU clocked at 2.00 GHz, 32GB memory and an NVIDIA GeForce GTX 1080 Ti GPU with 12GB VRAM. The scripts, configuration files, and resulting data files used in this study are available at: https://github.com/Budapest-Quantum-Computing-Group/hybrid_latent_qrl.

References

Martín Abadi, Paul Barham, Jianmin Chen, Zhifeng Chen, Andy Davis, Jeffrey Dean, Matthieu Devin, Sanjay Ghemawat, Geoffrey Irving, Michael Isard, Manjunath Kudlur, Josh Levenberg, Rajat Monga, Sherry Moore, Derek G. Murray, Benoit Steiner, Paul Tucker, Vijay Vasudevan, Pete Warden, Martin Wicke, Yuan Yu, and Xiaoqiang Zheng. TensorFlow: A system for Large-Scale machine learning. In *12th USENIX Symposium on Operating Systems Design and Implementation (OSDI 16)*, pages 265–283, Savannah, GA, November 2016.

USENIX Association. ISBN 978-1-931971-33-1. URL <https://www.usenix.org/conference/osdi16/technical-sessions/presentation/abadi>.

Eva Andrés, M. P. Cuéllar, and G. Navarro. Efficient dimensionality reduction strategies for quantum reinforcement learning. *IEEE Access*, 11:104534–104553, 2023. doi: 10.1109/ACCESS.2023.3318173.

Ville Bergholm, Josh Izaac, Maria Schuld, Christian Gogolin, Shahnawaz Ahmed, Vishnu Ajith, M. Sohaib Alam, Guillermo Alonso-Linaje, B. AkashNarayanan, Ali Asadi, Juan Miguel Arrazola, Utkarsh Azad, Sam Banning, Carsten Blank, Thomas R Bromley, Benjamin A. Cordier, Jack Ceroni, Alain Delgado, Olivia Di Matteo, Amintor Dusko, Tanya Garg, Diego Guala, Anthony Hayes, Ryan Hill, Aroosa Ijaz, Theodor Isacsson, David Ittah, Soran Jahangiri, Prateek Jain, Edward Jiang, Ankit Khandelwal, Korbinian Kottmann, Robert A. Lang, Christina Lee, Thomas Loke, Angus Lowe, Keri McKiernan, Johannes Jakob Meyer, J. A. Montañez-Barrera, Romain Moyard, Zeyue Niu, Lee James O’Riordan, Steven Oud, Ashish Panigrahi, Chae-Yeun Park, Daniel Polatajko, Nicolás Quesada, Chase Roberts, Nahum Sá, Isidor Schoch, Borun Shi, Shuli Shu, Sukin Sim, Arshpreet Singh, Ingrid Strandberg, Jay Soni, Antal Száva, Slimane Thabet, Rodrigo A. Vargas-Hernández, Trevor Vincent, Nicola Vitucci, Maurice Weber, David Wierichs, Roeland Wiersema, Moritz Willmann, Vincent Wong, Shaoming Zhang, and Nathan Killoren. PennyLane: Automatic differentiation of hybrid quantum-classical computations. *arXiv e-prints*, art. arXiv:1811.04968, November 2018. doi: 10.48550/arXiv.1811.04968.

- Kishor Bharti, Alba Cervera-Lierta, Thi Ha Kyaw, Tobias Haug, Sumner Alperin-Lea, Abhinav Anand, Matthias Degroote, Hermanni Heimonen, Jakob S Kottmann, Tim Menke, et al. Noisy intermediate-scale quantum algorithms. *Reviews of Modern Physics*, 94(1):015004, 2022.
- Samuel Yen-Chi Chen, Chih-Min Huang, Chia-Wei Hsing, Hsi-Sheng Goan, and Ying-Jer Kao. Variational quantum reinforcement learning via evolutionary optimization. *Machine Learning: Science and Technology*, 3(1):015025, feb 2022. doi: 10.1088/2632-2153/ac4559. URL <https://doi.org/10.1088%2F2632-2153%2Fac4559>.
- Zhengxue Cheng, Heming Sun, Masaru Takeuchi, and Jiro Katto. Deep Convolutional AutoEncoder-based Lossy Image Compression. *arXiv e-prints*, art. arXiv:1804.09535, April 2018. doi: 10.48550/arXiv.1804.09535.
- Rodrigo Coelho, André Sequeira, and Luís Paulo Santos. VQC-Based Reinforcement Learning with Data Re-uploading: Performance and Trainability. *arXiv e-prints*, art. arXiv:2401.11555, January 2024. doi: 10.48550/arXiv.2401.11555.
- Daoyi Dong, Chunlin Chen, Hanxiong Li, and Tzyh-Jong Tarn. Quantum reinforcement learning. *IEEE Transactions on Systems, Man, and Cybernetics, Part B (Cybernetics)*, 38(5):1207–1220, 2008. doi: 10.1109/TSMCB.2008.925743.
- Vedran Dunjko, Jacob M. Taylor, and Hans J. Briegel. Advances in quantum reinforcement learning. In *2017 IEEE International Conference on Systems, Man, and Cybernetics (SMC)*, pages 282–287, 2017. doi: 10.1109/SMC.2017.8122616.
- Ian Goodfellow, Yoshua Bengio, and Aaron Courville. Deep learning. *MIT Press*, pages 499–522, 2016.
- Casper Gyurik, Chris Cade, and Vedran Dunjko. Towards quantum advantage via topological data analysis. *Quantum*, 6:855, 2022.
- Danijar Hafner, Timothy Lillicrap, Jimmy Ba, and Mohammad Norouzi. Dream to Control: Learning Behaviors by Latent Imagination. *arXiv e-prints*, art. arXiv:1912.01603, December 2019. doi: 10.48550/arXiv.1912.01603.
- G. E. Hinton and R. R. Salakhutdinov. Reducing the dimensionality of data with neural networks. *Science*, 313(5786):504–507, jul 2006. doi: 10.1126/science.1127647. URL <https://doi.org/10.1126/science.1127647>.
- Hsin-Yuan Huang, Michael Broughton, Jordan Cotler, Sitan Chen, Jerry Li, Masoud Mohseni, Hartmut Neven, Ryan Babbush, Richard Kueng, John Preskill, et al. Quantum advantage in learning from experiments. *Science*, 376(6598):1182–1186, 2022.
- Norman P. Jouppi, George Kurian, Sheng Li, Peter Ma, Rahul Nagarajan, Lifeng Nai, Nishant Patil, Suvinay Subramanian, Andy Swing, Brian Towles, Cliff Young, Xiang Zhou, Zongwei Zhou, and David Patterson. TPU v4: An Optically Reconfigurable Supercomputer for Machine Learning with Hardware Support for Embeddings. *arXiv e-prints*, art. arXiv:2304.01433, April 2023. doi: 10.48550/arXiv.2304.01433.
- Nathan Killoran, Thomas R. Bromley, Juan Miguel Arrazola, Maria Schuld, Nicolás Quesada, and Seth Lloyd. Continuous-variable quantum neural networks. *Phys. Rev. Res.*, 1:033063, Oct 2019. doi: 10.1103/PhysRevResearch.1.033063. URL <https://link.aps.org/doi/10.1103/PhysRevResearch.1.033063>.
- Diederik P. Kingma and Max Welling. Auto-encoding variational bayes. *CoRR*, art. arXiv:1312.6114, 2013.
- Diederik P. Kingma and Max Welling. An Introduction to Variational Autoencoders. *arXiv e-prints*, art. arXiv:1906.02691, June 2019. doi: 10.48550/arXiv.1906.02691.
- Zoltán Kolarovszki, Tomasz Rybotycki, Péter Rakyta, Ágoston Kaposi, Boldizsár Poór, Szabolcs Jóczik, Dániel T. R. Nagy, Henrik Varga, Kareem H. El-Safty, Gregory Morse, Michał Oszmaniec, Tamás Kozsik, and Zoltán Zimborás. Piquasso: A Photonic Quantum Computer Simulation Software Platform. *arXiv e-prints*, art. arXiv:2403.04006, March 2024. doi: 10.48550/arXiv.2403.04006.
- Yunseok Kwak, Won Joon Yun, Soyi Jung, Jong Kook Kim, and Joongheon Kim. Introduction to quantum reinforcement learning: Theory and pennylane-based implementation. In *ICTC 2021 - 12th International Conference on ICT Convergence*, International Conference on ICT Convergence, pages 416–420. IEEE Computer Society, 2021. doi: 10.1109/ICTC52510.2021.9620885. Funding Information: ACKNOWLEDGMENT This work was supported by

- the National Research Foundation of Korea (2019M3E4A1080391). Joongheon Kim is a corresponding author of this paper. Publisher Copyright: © 2021 IEEE.; 12th International Conference on Information and Communication Technology Convergence, ICTC 2021 ; Conference date: 20-10-2021 Through 22-10-2021.
- Lucas Lamata. Quantum reinforcement learning with quantum photonics. *Photonics*, 8(2), 2021. ISSN 2304-6732. doi: 10.3390/photonics8020033. URL <https://www.mdpi.com/2304-6732/8/2/33>.
- Sascha Lange and Martin A. Riedmiller. Deep auto-encoder neural networks in reinforcement learning. *The 2010 International Joint Conference on Neural Networks (IJCNN)*, pages 1–8, 2010.
- Jonathan Wei Zhong Lau, Kian Hwee Lim, Harshank Shrotriya, and Leong Chuan Kwek. Nisq computing: where are we and where do we go? *AAPPS bulletin*, 32(1):27, 2022.
- Ji-An Li, Daoyi Dong, Zhengde Wei, Ying Liu, Yu Pan, Franco Nori, and Xiaochu Zhang. Quantum reinforcement learning during human decision-making. *Nature human behaviour*, 4(3): 294–307, 2020.
- Xiao-Jiao Mao, Chunhua Shen, and Yu-Bin Yang. Image Restoration Using Convolutional Auto-encoders with Symmetric Skip Connections. *arXiv e-prints*, art. arXiv:1606.08921, June 2016. doi: 10.48550/arXiv.1606.08921.
- Nico Meyer, Christian Ufrecht, Maniraman Periyasamy, Daniel D Scherer, Axel Plinge, and Christopher Mutschler. A survey on quantum reinforcement learning. *arXiv preprint arXiv:2211.03464*, 2022.
- D. Nagy, Z. Tabi, P. Haga, Z. Kallus, and Z. Zimboras. Photonic quantum policy learning in openai gym. In *2021 IEEE International Conference on Quantum Computing and Engineering (QCE)*, pages 123–129, Los Alamitos, CA, USA, oct 2021. IEEE Computer Society. doi: 10.1109/QCE52317.2021.00028. URL <https://doi.ieeecomputersociety.org/10.1109/QCE52317.2021.00028>.
- Egor E. Nuzhin and Dmitry Yudin. Quantum-enhanced policy iteration on the example of a mountain car, 2023.
- Adrián Pérez-Salinas, Alba Cervera-Lierta, Elies Gil-Fuster, and José I Latorre. Data re-uploading for a universal quantum classifier. *Quantum*, 4:226, 2020.
- Francisco Restrepo, Junjing Zhao, and Utpal Chatterjee. Denoising and feature extraction in photoemission spectra with variational auto-encoder neural networks. *Review of Scientific Instruments*, 93(6):065106, 06 2022. ISSN 0034-6748. doi: 10.1063/5.0090051. URL <https://doi.org/10.1063/5.0090051>.
- Albert Reuther, Peter Michaleas, Michael Jones, Vijay Gadepally, Siddharth Samsi, and Jeremy Kepner. AI and ML Accelerator Survey and Trends. *arXiv e-prints*, art. arXiv:2210.04055, October 2022. doi: 10.48550/arXiv.2210.04055.
- Diego Ristè, Marcus P Da Silva, Colm A Ryan, Andrew W Cross, Antonio D Córcoles, John A Smolin, Jay M Gambetta, Jerry M Chow, and Blake R Johnson. Demonstration of quantum advantage in machine learning. *npj Quantum Information*, 3(1):16, 2017.
- Robin Rombach, Andreas Blattmann, Dominik Lorenz, Patrick Esser, and Björn Ommer. High-resolution image synthesis with latent diffusion models. In *2022 IEEE/CVF Conference on Computer Vision and Pattern Recognition (CVPR)*, pages 10674–10685, 2022. doi: 10.1109/CVPR52688.2022.01042.
- Valeria Saggio, Beate E Asenbeck, Arne Hamann, Teodor Strömberg, Peter Schiansky, Vedran Dunjko, Nicolai Friis, Nicholas C Harris, Michael Hochberg, Dirk Englund, et al. Experimental quantum speed-up in reinforcement learning agents. *Nature*, 591(7849):229–233, 2021.
- Antonio Sanna, Andrea Giordano, N Lo Gullo, Carlo Mastroianni, and Francesco Plastina. A hybrid classical-quantum approach to speed-up q-learning. *Scientific Reports*, 13(1):3913, 2023.
- Michael Schenk, Elías F Combarro, Michele Grossi, Verena Kain, Kevin Shing Bruce Li, Mircea-Marian Popa, and Sofia Vallecora. Hybrid actor-critic algorithm for quantum reinforcement learning at cern beam lines. *Quantum Science and Technology*, 9(2):025012, feb 2024. doi: 10.1088/2058-9565/ad261b. URL <https://dx.doi.org/10.1088/2058-9565/ad261b>.
- Maria Schuld, Alex Bocharov, Krysta M. Svore, and Nathan Wiebe. Circuit-centric quantum classifiers. *Physical Review A*, 101(3), March 2020. ISSN 2469-9934. doi: 10.1103/physreva.101.032308. URL <http://dx.doi.org/10.1103/PhysRevA.101.032308>.

- John Schulman, Sergey Levine, Pieter Abbeel, Michael Jordan, and Philipp Moritz. Trust region policy optimization. In Francis Bach and David Blei, editors, *Proceedings of the 32nd International Conference on Machine Learning*, volume 37 of *Proceedings of Machine Learning Research*, pages 1889–1897, Lille, France, 07–09 Jul 2015. PMLR. URL <https://proceedings.mlr.press/v37/schulman15.html>.
- John Schulman, Filip Wolski, Prafulla Dhariwal, Alec Radford, and Oleg Klimov. Proximal policy optimization algorithms, 2017.
- John Schulman, Philipp Moritz, Sergey Levine, Michael Jordan, and Pieter Abbeel. High-dimensional continuous control using generalized advantage estimation, 2018.
- Richard S. Sutton, David McAllester, Satinder Singh, and Yishay Mansour. Policy gradient methods for reinforcement learning with function approximation. In *Proceedings of the 12th International Conference on Neural Information Processing Systems, NIPS'99*, page 1057–1063, Cambridge, MA, USA, 1999. MIT Press.
- Neil C. Thompson, Kristjan Greenewald, Keeheon Lee, and Gabriel F. Manso. The Computational Limits of Deep Learning. *arXiv e-prints*, art. arXiv:2007.05558, July 2020. doi: 10.48550/arXiv.2007.05558.
- Mark Towers, Jordan K. Terry, Ariel Kwiatkowski, John U. Balis, Gianluca de Cola, Tristan Deleu, Manuel Goulão, Andreas Kallinteris, Arjun KG, Markus Krimmel, Rodrigo Perez-Vicente, Andrea Pierré, Sander Schulhoff, Jun Jet Tai, Andrew Tan Jin Shen, and Omar G. Younis. Gymnasium, March 2023. URL <https://zenodo.org/record/8127025>.
- Herke van Hoof, Nutan Chen, Maximilian Karl, Patrick van der Smagt, and Jan Peters. Stable reinforcement learning with autoencoders for tactile and visual data. In *2016 IEEE/RSJ International Conference on Intelligent Robots and Systems (IROS)*, pages 3928–3934, 2016. doi: 10.1109/IROS.2016.7759578.
- Pascal Vincent, Hugo Larochelle, Yoshua Bengio, and Pierre-Antoine Manzagol. Extracting and composing robust features with denoising autoencoders. In *Proceedings of the 25th International Conference on Machine Learning, ICML '08*, page 1096–1103, New York, NY, USA, 2008. Association for Computing Machinery. ISBN 9781605582054. doi: 10.1145/1390156.1390294. URL <https://doi.org/10.1145/1390156.1390294>.
- Shaojun Wu, Shan Jin, Dingding Wen, Donghong Han, and Xiaoting Wang. Quantum reinforcement learning in continuous action space. *arXiv e-prints*, art. arXiv:2012.10711, December 2020. doi: 10.48550/arXiv.2012.10711.
- Tailong Xiao, Xinliang Zhai, Xiaoyan Wu, Jianping Fan, and Guihua Zeng. Practical advantage of quantum machine learning in ghost imaging. *Communications Physics*, 6(1):171, 2023.
- Lev Yassenko, Yaroslav Klyatchenko, and Oksana Tarasenko-Klyatchenko. Image noise reduction by denoising autoencoder. In *2020 IEEE 11th International Conference on Dependable Systems, Services and Technologies (DESSERT)*, pages 351–355, 2020. doi: 10.1109/DESSERT50317.2020.9125027.
- Yu Yu, Weibin Zhang, and Yun Deng. Frechet inception distance (fid) for evaluating gans. *China University of Mining Technology Beijing Graduate School: Beijing, China*, 2021.
- Nikola Zubić, Federico Soldá, Aurelio Sulser, and Davide Scaramuzza. Limits of Deep Learning: Sequence Modeling through the Lens of Complexity Theory. *arXiv e-prints*, art. arXiv:2405.16674, May 2024. doi: 10.48550/arXiv.2405.16674.